Journal of Energy Storage 104 (2024) 114495

Contents lists available at ScienceDirect

Journal of Energy Storage

journal homepage: www.elsevier.com/locate/est

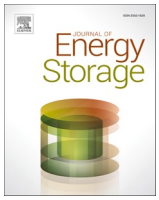

Research papers

Self-heating performance of phase change cementitious mortar with hybrid carbon-based nanomaterials

Xiaonan Wang [a,b], Yipu Guo [b], Zhong Tao [c], Long Shi [d], Wengui Li [b,*]

[a] Shool of Civil and Environmental Engineering, University of Technology Sydney, NSW 2007, Australia
[b] Centre for Infrastructure Engineering and Safety, School of Civil and Environmental Engineering, The University of New South Wales, NSW 2052, Australia
[c] Centre for Infrastructure Engineering, Western Sydney University, NSW 2751, Australia
[d] State Key Laboratory of Fire Science, University of Science and Technology of China, Hefei 230026, China

ARTICLE INFO

Keywords:
Phase change material (PCM)
Self-heating
Carbon black
Carbon nanotube
Energy saving

ABSTRACT

Temperature fluctuations pose a critical challenge for infrastructure, necessitating functional concrete to protect structures and promote sustainability. Self-heating concrete and phase change material (PCM) concrete are closely linked to thermal energy, with the former focused on heat generation and the latter on heat storage. This study aims to explore the self-heating performance of modified PCM concrete. Carbon-based materials, chosen for their low electrical resistance and high thermal conductivity, are incorporated to enhance the PCM concrete. Carbon black (CB), carbon nanotubes (CNT), and carbon fibres (CF) with various dimensions and scales, are combined to achieve optimal performance. Materials below a threshold yield minimal change, as they fail to establish the crucial conductive circuit. The self-heating behaviour becomes pronounced with increased in materials, reaching an optimal temperature rise up to 31.2 °C in one hour. However, the group with the highest content of materials experiences a reduced final temperature of 23.9 °C and an increased electrical conductivity of 40 Ω. CB and CNT show different efficiency improvements, and the ideal combination is proposed as 0.3 % CNT and 0.75 % CB. Inorganic hydrated salt-based PCM reduces electrical conductivity by 12 % – 35 % in its liquid state due to free ions, potentially enhancing self-heating capability, though its impact is less significant compared to carbon materials. Overall, the optimum group demonstrates significant self-heating behaviour, high efficiency, and low material cost. Models and electrical impedance results validate these observations and provide novel insight into the self-heating performance of PCM mortar with hybrid carbon-based materials.

1. Introduction

In modern development, infrastructure meets various challenges, and advanced building materials are continually proposed. Self-heating concrete is electrically conductive and aims to raise the temperature of the concrete by current application. Ice removal is one of the significant advantages [1] (such as in pavement systems [2]) and achieving further benefits (like modifying curing conditions [3]) is also favourable. A self-heating concrete with a low cost can show an impressive ice-melting capacity. A heating rate of 0.05 °C/min was able to melt the ice with a thickness of 6 mm in less than 4 h [4]. It is noticeable that the experiment was done at −15 °C costing an energy consumption of only 4.3 kWh/m^2. Furthermore, an increase of 19 % in flexural strength was observed due to the inclusion of the conductive fibres [4]. The potential of self-heating concrete is huge and valuable for advanced construction.

First of all, the achievement of self-heating concrete demands the generation of electrically conductive paths, which is a challenge for conventional concrete. Most researchers prefer to use conductive additives to improve the electrical conduction of concrete. Metal-based materials are common electrically conductive choices and have shown significant performance in self-heating concrete [3,5]. Moreover, carbon-based materials are dominant in improving the self-heating ability of concrete [6–8]. Additionally, nanomaterials are introduced in concrete and present amazing results when the nano-carbons, typically CNT and CB, are selected to fabricate electrical conduction paths. For example, CNT has attracted much attention in concrete development as well as self-heating. Kim et al. [9] proved the remarkable self-heating ability. Great stability and strength preservation of the re-heating cycle were presented at a lower content of CNT. The incorporation method is far more than a direct addition of CNT solution. Lee et al. [10] proposed

* Corresponding author at: School of Civil and Environmental Engineering, The University of New South Wales, NSW 2052, Australia.
E-mail address: wengui.li@unsw.edu.au (W. Li).

https://doi.org/10.1016/j.est.2024.114495
Received 21 June 2024; Received in revised form 30 September 2024; Accepted 1 November 2024
Available online 11 November 2024

a CNT-coated film that was inserted in the middle of the sample. The highest heating result and lowest electrical resistance were observed if both CNT incorporation methods were used. Compared to the addition of CNT solution, the concentrated CNT of film generated a much higher heating performance. Longer curing time improved the efficiency, but the influence was slight. Jang et al. [11] proposed that the incorporation of silica aerogel enhanced the heating performance of CNT-based self-heating concrete. The high hydrophobicity of silica aerogel protected the CNT from water ingress, providing higher and more reliable thermal conductivity. CB is another popular carbon additive for functional concrete and the concrete type is not limited to conventional Portland cement-based concrete. CB showed great improvement in electrical conductivity with great mechanical properties of geopolymer concrete. A temperature increase of 20–31 °C was achieved in 2 h [12]. The percolation threshold of carbon black (CB) in geopolymer concrete was determined to be 1.5 wt%, with the self-heating performance enhancing as the CB content increased [13]. Higher voltage boosted better heating power, compensating for the weak efficiency at a low CB dosage. An efficient configuration application can improve the performance more ideally [14].

Many experiments have been conducted to explore methods with higher effectiveness and sustainability. A combination of different additives is popular. Farcas et al. [15] prepared conductive concrete using CNT and graphite powder (GP). An excellent self-heating result was obtained at both AC (alternating current) and DC (direct current) voltage. An increase of 50 °C was achieved at 40 V in this experiment. In addition, the application of 65 V was proposed to stop ice formation with little energy consumption. Gwon et al. [16] proved the benefit of CB on the self-heating capacity of CF-based cement paste. The CF/CB-based cement paste sample with the highest conductivity provided obvious porosity reduction and more hydration products at the constant voltage. The effective electrical conductivity and temperature rising were illustrated with the help of CB addition up to 8 vol%. The excessive CB caused agglomeration, leading to lower efficiency. The lower compressive strength was distinct due to the low density of carbon addition and increased w/c ratio. They [17] also revealed the effects of various curing conditions on self-heating performance. The reason was explained by the changed structure and hydration level that influenced the electrical resistivity. The oven-cured samples showed longer periods of self-heating capacity. It can be derived from current research that the physical properties with various dimensions have intrinsic features for conductive path generation in different aspects, like the path length and distribution quality. A proper combination could be helpful for a stable conductive path in concrete.

Multifunctional concrete prevails in smart city development since the challenges faced by buildings are diverse. It is possible for self-heating concrete to achieve multiple functions. Wang et al. [18] calcinated magnetically separated fly ash to produce conductive aggregates and cast mortar with CF. The highest temperature achieved was 90 °C for the mortar at 8 V DC, and the Seebeck coefficient was greater than 2.63 mV/°C. The electrical heating performance of the mortar was reliable and can be used as a thermal sensor. Abedi et al. [19] designed smart planar composites by coating CNT/graphene nanoplatelet (GNP) on fabrics (immersed in diluted H_2SO_4 solutions in advance) via the screen-printing method. A thermoplastic polyurethane layer was coated as the outermost shell, providing protection and waterproofing. Under 25 V DC application, a heating rate of 0.44 °C/s and joule heating power of 0.7 W/°C were obtained, and the sample reached the maximum temperature of 44 °C. The high sensitivity of piezoelectricity and improved flexural strength were also evident in the prepared sample.

Concrete with the inclusion of PCM is a prominent option, which can be a beneficial solution for avoiding freeze-thaw damage [20], achieving comfortable room temperature [21,22], energy saving and pollution reduction [23,24], etc. PCM concrete is a prevailing topic for energy-saving that can store thermal energy [25–27]. Improper thermal conductivity is a universal problem of PCM efficiency, and researchers have paid much attention to it. Carbon and metal-based materials are commonly used to solve this issue [28,29]. Fortunately, the carbon additives mentioned in the previous paragraph for self-heating concrete development are also critical for the efficiency improvement in PCM concrete [30], which promotes the cooperation of self-heating and PCM concrete. In summary, achieving self-heating capability in modified PCM concrete could be feasible.

A few attempts have been reported to develop PCM concrete with self-heating ability. Jang et al. [31] added various amounts of PCM to self-heating paste with 0.8 wt% CNT and 0.2 wt% CF. The selected PCM was capsulised paraffin-based material. A higher content of PCM decreased the electrical conductivity and compressive strength, negatively influencing the samples' self-heating capacity. A lower cooling speed and greater heat storage were observed. This experiment illustrated the possibility of adding PCM to self-heating concrete, but further research was required to improve the comprehensive performance. Niu et al. [32] tested the heat storage of PCM composite while a built-in electrical heating device was used. The relationship between thermal conductivity and heating power was investigated, which proved the potential of electrical heating to provide thermal power for energy storage.

As far as we know, the self-heating concrete with PCM has not shown amazing heating efficiency. The compatibility has not been explained well, especially regarding the effect of PCM addition on self-heating performance. Moreover, the optimal generation of conductive paths for self-heating concrete is still unclear. Therefore, this study aims to explore the self-heating capability of modified PCM concrete in order to help improve the comprehensive ability of the multifunctional concrete and provide important suggestions. Carbon additives are beneficial to the efficiency of PCM concrete and critical to the conductive path of self-heating concrete [33,34] and the combination could be a preferred method. Three carbon additives are incorporated with various amounts in a hydrated inorganic salt-based PCM mortar. The effect of additives' properties (like shape, size, etc.) is analysed, which attempts to take full advantage of multi-scale additives for more attributive performance [33]. Self-heating capability is evaluated by temperature distribution and increment under constant DC voltage, in addition to the key parameter of electrical conductivity. FTIR, SEM, and electrical impedance techniques are used to analyse the inner differences and explain the changing self-heating capability. The sensitivity of raw nanocarbon additives is also calculated, and the optimal mix design is proposed. The effect of PCM on electrical properties and self-heating ability is proven. This work will promote multifunctional PCM concrete with self-heating ability.

2. Material and preparation

Mixing proportions of a total of 10 mixes are shown in Table 1. The water-to-cement ratio was kept at 0.46 while the superplasticiser (SP)-to-cement ratio varied from 0.5 % to 4.5 % to adjust the flowability. Expanded perlite (EP, with a high porosity of 65 %) was selected as support material to absorb PCM as PCM composite and aggregate

Table. 1
Mix proportions for all samples.

Name	Cement	Water	SS	EPC	SP	CNT	CF	CB
T0B0	2100	966	2100	336	3.5	0	0	0
T1B25	2100	966	2100	336	21	0.7	3.5	1.75
T3B25	2100	966	2100	336	24.5	2.1	3.5	1.75
T5B25	2100	966	2100	336	28	3.5	3.5	1.75
T1B5	2100	966	2100	336	21	0.7	3.5	3.5
T3B5	2100	966	2100	336	24.5	2.1	3.5	3.5
T5B5	2100	966	2100	336	31.5	3.5	3.5	3.5
T1B75	2100	966	2100	336	21	0.7	3.5	5.25
T3B75	2100	966	2100	336	28	2.1	3.5	5.25
T5B75	2100	966	2100	336	31.5	3.5	3.5	5.25

[35,36]. All samples had the same proportion of EP-based PCM composite (EPC). Analytical reagents of $Na_2HPO_4{\cdot}12H_2O$ and $Na_2SO_4{\cdot}10H_2O$ were selected as core PCMs [37]. To fabricate EPC, the same amounts of the two PCMs were melted and mixed at 60 °C in advance before being impregnated in EP at 50 °C with a vacuum pressure of 80 kPa. After impregnation, EPC was discretely placed on a piece of absorbent paper as one layer and covered by another piece with gentle pressure. The EPC and paper were stored at 50 °C and 80 kPa for 24 h, which kept PCM in liquid. The EPC size of around 1 mm allowed a minor surface gap between EPC and paper. The most liquid PCM on the EPC surface will be absorbed by the paper. The mass ratio of EP to PCM was 0.6. After four hours, the composite was naturally cooled to room temperature and taken out, completing EPC fabrication. As reviewed in the introduction section, conductive fillers with various sizes have obvious differences in building the conductive path. The gradient scales and shapes may cooperate effectively, so three carbon-based materials (CNT, nano CB, and millimetre CF) with remarkable features were selected. The sample name in Table 1 illustrates the content of carbon additives. Taking T3B25 as an example, the mass ratio of CNT to cement was 0.3 %, and the CB counterpart was 0.25 %. The CF percentage was 0.5 % in most samples except T0B0. CF was manually dispersed from the cluster as separated fibres and mixed with dry materials (cement, sand, EPC) for 20 min at low speed. The nanomaterials CB and CNT were mixed in water with SP in advance, followed by ultrasonic wave dispersion for 30 min. Then, the nanomaterial suspension was added to a mixing pot with dry materials. The time gap between the ultrasonic dispersion end and final mixing in the pot was controlled in less than 5 min. The freshly mixed material was cast in cubic moulds of size 50 × 50 × 50 mm [38]. Stable conductive electrodes were essential for self-heating tests, and copper mesh was recommended [33,39]. Two pieces of copper mesh, with a dimension of 25 × 45 mm, were embedded in each specimen as electrodes. A part of the electrode was inserted in a fresh mortar cube with a depth of 35 mm, which provided a large contact area with the mortar. The rest part allowed the connection with the power supplier. A gap of 30 mm was kept between the two electrodes. The electrode distribution was centrosymmetric, and the parameters are shown in Fig. 1. The cast samples were covered by plastic film to eliminate moisture evaporation for one day. Then, demoulded samples were kept in a curing chamber (24 °C and humidity of 95 %) until the 28th day.

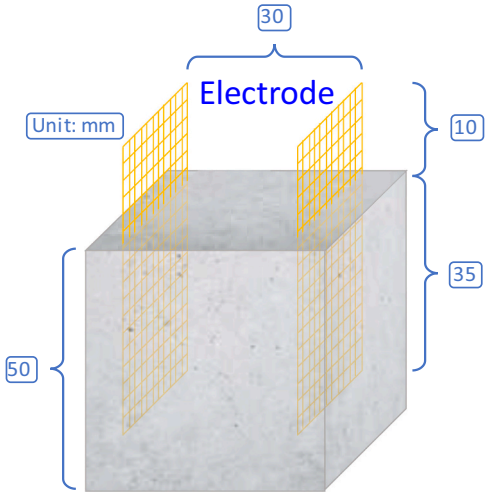

Fig. 1. Diagram of specimens with copper electrodes.

3. Methodology

3.1. Self-heating performance under DC

All prepared samples had two electrodes that were connected to the power supply. The input standard Australian power, 240 V AC 50 Hz was transferred to DC. The output voltage was set to 10 V. A handheld infrared thermometer was used to capture the temperature distribution and changes, which was manufactured by HIKMICRO Sensing Technology Co., Ltd. The testing distance was 0.5 m, and the room temperature was ~23 °C. A rough layer was placed under the sample to remove the infrared reflection caused by the flat table. The recording started once the current was applied. Every test costs about one hour. The test configuration is shown in Fig. 2.

3.2. Electrical resistance (conductivity)

The electrical resistance is a critical factor in the assessment of self-heating concrete. A multimeter with a maximum value of 200 kΩ was used to test the electrical resistance. Probes were connected to the electrodes of the samples. The tests were repeated five times, and the average values were determined. Apart from the electrical resistance at room temperature (~23 °C), the samples were heated at 60 °C in an oven for 4 h to measure the electrical resistance at high temperatures. An insulative table and a conductive layer were used to eliminate interference. All samples were stored in sealed containers before conducting the experiment.

3.3. Fourier transform infrared spectroscopy

Fourier Transform Infrared Spectroscopy (FTIR) is the main technique used to quickly analyse the chemical composition of cement composites. A Perkin Elmer Frontier IR spectrophotometer was used in this experiment with an absorption spectrum range of 4000–400 cm^{-1} and a resolution of 2 cm^{-1}. The testing range can meet the common requirement for the cement-based composite material that incorporates hydrated inorganic salt and carbon additives. The number of measuring circles was 30 times to guarantee the accuracy of the results. The facility will provide the final result automatically after processing the circles. All samples were ground as fine powders and sealed in tubes. The test was completed in dry laboratory conditions to eliminate the influence of ambient moisture.

3.4. Microstructure

Scanning Electron Microscope (SEM) was a popular method to capture the microstructure performance of materials. Considering the scale of nano additives and cement hydration products, Zeiss Supra 55VP SEM was used in this experiment with a maximum magnification of over 80 k. The resolution can reach 1 nm at the accelerating voltage of 5 kV with the detector of In-lens. A gold layer with a thickness of 10 nm was coated by Leica EM ACE600 Coater to form a conductive path. All samples were stored in a vacuum desiccator to prevent moisture and dust from the air.

3.5. Electrical impedance

AC impedance spectroscopy is proposed to investigate the microstructure and conductive pathway of cement-based materials, which is non-destructive and effective [33]. Two probe methods were adopted considering their reliability. The tests were performed at room temperature (23 °C) and temperature above the phase change point of PCM (60 °C). For the test at 60 °C, the specimens were placed in a 60 °C oven for 3 h and then tested immediately. The data was tested via AMETEK 1260 A Impedance/Gain-Phase Analyzer, which had a wide frequency ranging from 32 MHz to 10 μHz with 0.015 ppm resolution. The spectrum results were analysed using the equivalent circuit method of ZView

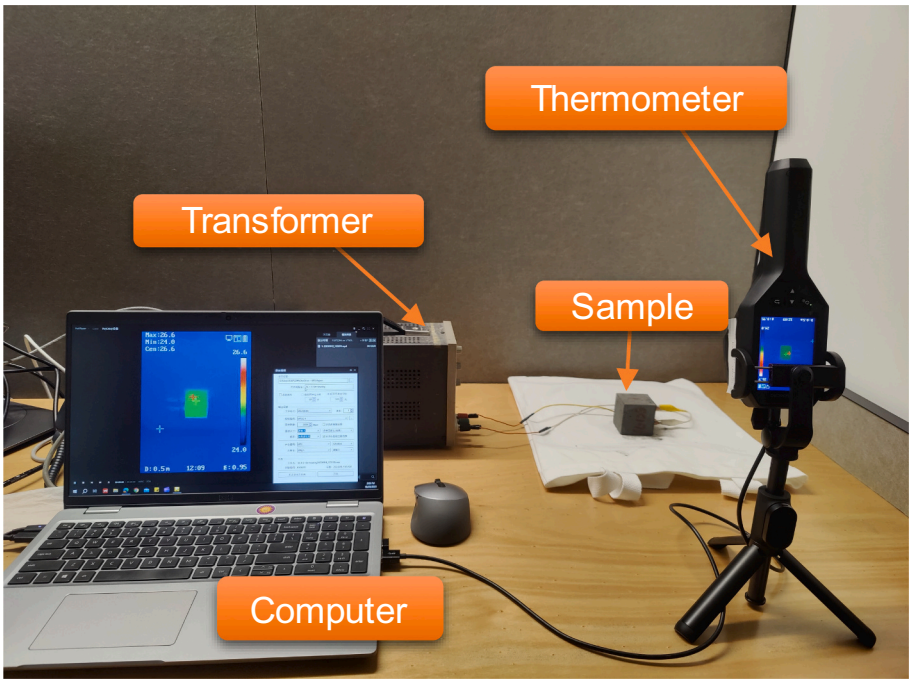

Fig. 2. Configuration of self-heating concrete test.

software.

4. Results and discussion

4.1. Self-heating performance under DC

4.1.1. Surface temperature distribution

The initial temperature distribution is shown in Fig. 3. All maps had the same temperature legend that was placed on the left. The two-end temperatures were marked on the map. The "cen" temperature was the central point temperature of the green "+". The maximum temperature point was observed on the insulating cover of electrodes caused by manual operation (e.g., T1B25), which did not affect the temperature distribution of samples. The surface temperature of the samples was close to the environmental temperature, as shown in Fig. 3.

A temperature hike appeared in Fig. 4 after applying current for 10 min. Compared with the initial temperatures, the temperature increases in T0B0, T1B25, and T1B5 was negligible. The content of additives failed to build a strong electrically conductive path. A remarkable temperature increase was found in T1B75, which can be defined as the threshold. Most parts in the sample reached over 25 °C. T3B25 showed similar results with moderately higher temperatures. The temperature

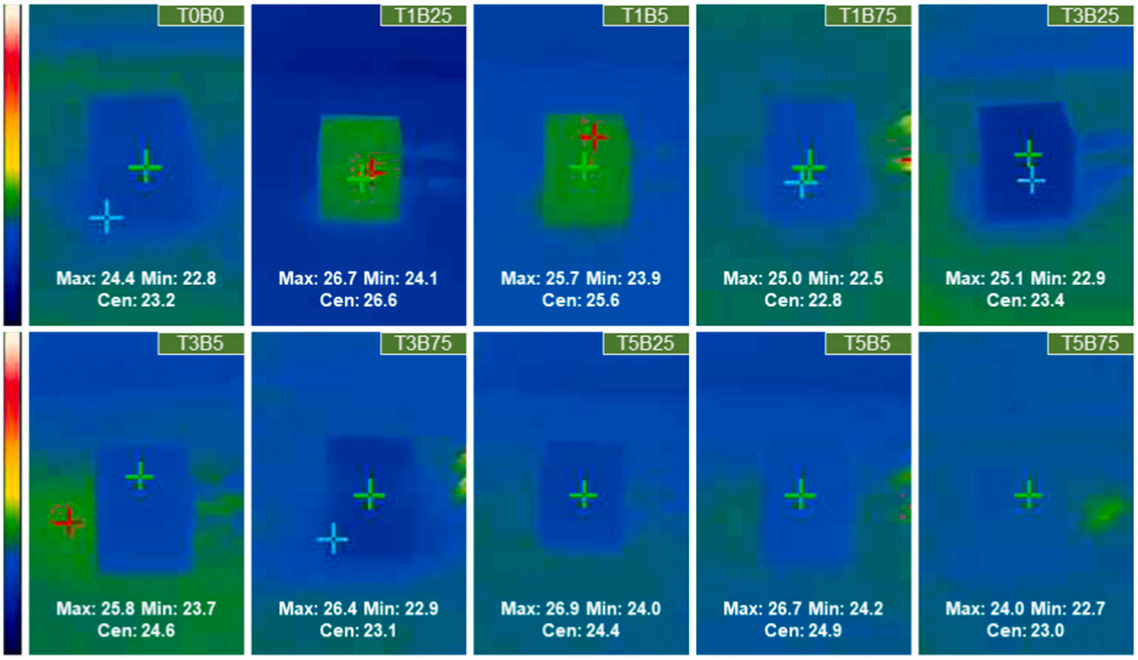

Fig. 3. Initial state of samples before test.

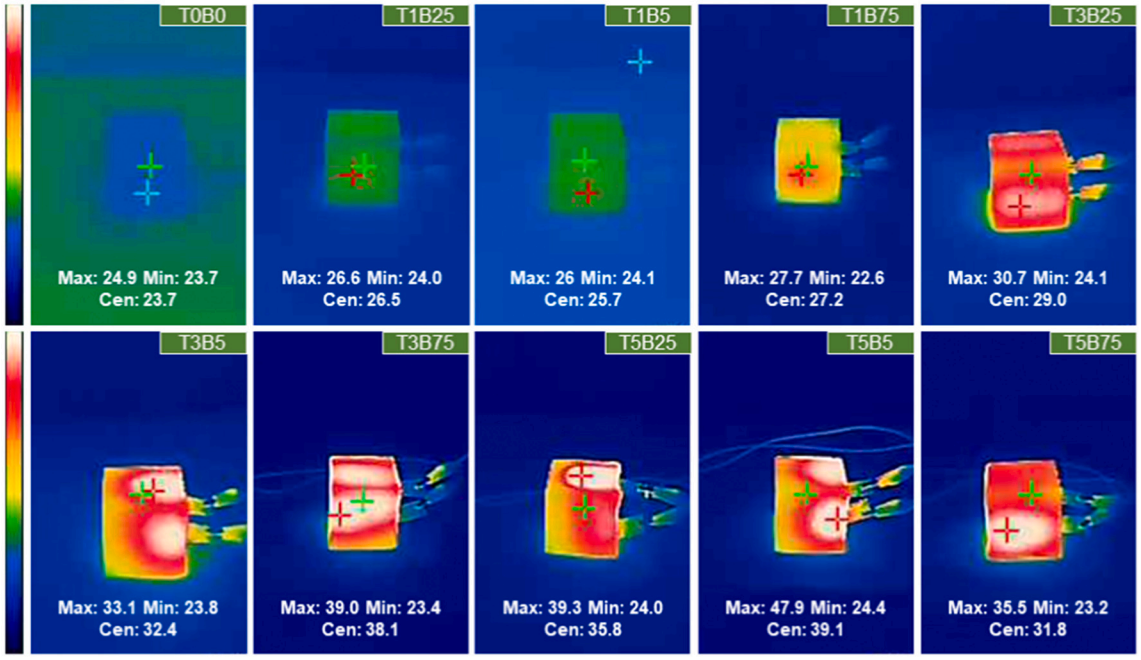

Fig. 4. Temperature distribution at 10 min after current application.

distribution of T1B75 and T3B25 was generally uniform because the low electrical conductivity led to a moderate heating rate. The carbon addition provided better heating efficiency when the maximum value was observed in T5B5 (rocketed to 47.9 °C). The evident temperature gradient occurred from T3B5 to T5B75 with the rough gaps of 5, 8, 8, 12, and 6 °C, respectively. This rank also agreed with a temperature rise, which was caused by the various heating rates. The area close to the electrodes was hotter and showed an oval boundary. This was caused by the stronger current near the electrodes.

The temperature in most samples rose further after applying current for 30 min, as shown in Fig. 5. The non-conductive samples presented no change. The uneven temperature distribution appeared in T1B75 and T3B25 with the difference of ~2 °C and ~ 3 °C, caused by the heat accumulation. The regulation was similar to other conductive samples. From T3B5 to T5B75, the temperature distribution was maintained, but the value was higher. T5B5 was still on the top of the list (maximum value up to 63.5 °C, and the central point reached 54.1 °C). In addition, the temperature gradients were relatively decreased compared to Fig. 4, which declined to around 4, 7, 6.5, 10 and 6 °C, respectively. Higher maximum temperatures still synchronized with higher gradients, which were strongly attributed to the heating generation rate. According to Fourier's law, the temperature difference between the samples and the room became larger with time, which contributed to faster heat loss.

After one hour of current application, the temperature maps were

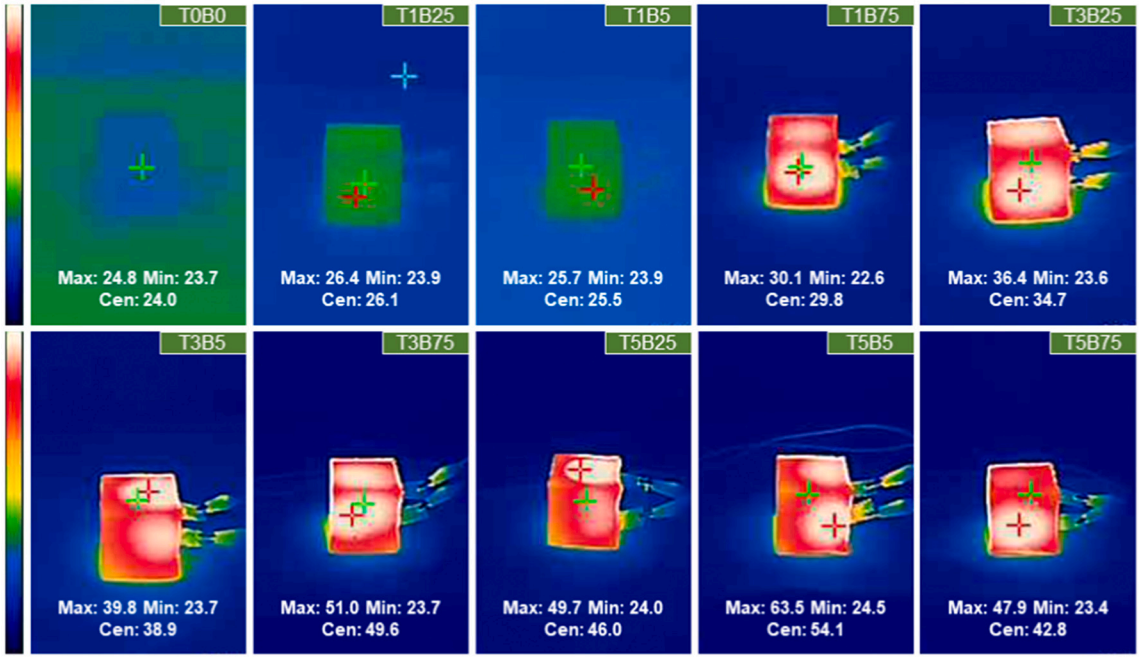

Fig. 5. Temperature distribution at 30 min after current application.

recorded, as shown in Fig. 6. The current application did not change the conductivity, and no self-heating was observed from T0B0 to T1B5. The increase was weaker for conductive samples, especially for T1B75 (even showing a minor decrease) and T3B25. The main features of temperature distribution in Fig. 5 were kept while the T1B75 changed to uniform. Higher temperatures were still concentrated near the electrodes, where the most heat was generated, as shown in Fig. 4, and the rest of the areas tended to release heat. The similar temperature distribution was caused by the balance of heat generation and loss. The stable states were approached after one-hour current application, while the temperature gradients were maintained at about 4, 7, 7, 10 and 6 °C, respectively. The changes compared to Fig. 5 were very limited. In this case, the results in Fig. 6 were regarded as the final stable state, which approached the highest temperature in this experiment.

4.1.2. Temperature development of the central point in thermal maps

To reveal the heating performance with time, the temperature development of the central point and first-order derivative curve were plotted in Fig. 7. The T was recorded as the temperature difference to the initial value that eliminated the slightly various room temperatures. According to the results, most samples showed obvious temperature climbing except T0B0, T1B25 and T1B5, where the conductive path was not built, as explained in Fig. 4 [9]. The increasing trend went minor with time but showed different heating results. All samples reached stable after one hour. Generally, the higher content of carbon additives led to higher temperatures. T5B5 presented the highest value, and samples with T5 occupied 3 seats of the top 4 samples. T5B75 did not provide the best self-heating performance as expected, which was even worse than T5B25. The superfluous nano-additives were prone to cause agglomeration that could hinder a uniform conductive path generation [6].

The self-heating efficiency is shown in Fig. 7 (b) by the first-order derivative. The heating rate moderately dropped with time, although a slight increment was observed in T3B25, T5B5, and T5B75. The ionic polarisation at the first current application can explain this exception. The value rank at 10 min in Fig. 7 (b) was in accord with the final value rank in Fig. 7 (a). T1B75 presented zero increment firstly among conductive samples at 30 min. The rate of T5B5 fell to zero at 45 min that was similar to T3B25 and T3B5, even though the final temperature was much higher. T3B75, T5B25, and T5B75 showed better sustainable self-heating that was prolonged to 55 min.

4.1.3. Assessment of conductive additives

The expected critical assessment index, i.e., maximum temperature increment, was plotted in Fig. 8. The gap between the top 2 samples, T5B5 and T3B75, was negligible. T5B25 and T5B75 followed the top 2 samples, and the decrease was very limited. The advantages of the top 4 were remarkable, which doubled the performance of the rest of the samples. These samples used varying CNT and CB contents with constant CF. The effectiveness of different additives cannot be simply reflected by the maximum temperature increment.

The various material mixing plans influenced the improvement of efficiency. To explore the efficiency of different carbon materials, the electrical sensitivities of CNT and CB are defined as shown in Eqs. (1) and (2).

$$S_{CNT} = \Delta T / M_{CNT} \tag{1}$$

$$S_{CB} = \Delta T / M_{CB} \tag{2}$$

where S_{CNT} and S_{CB} are the electrical sensitivity of CNT and CB, respectively; ΔT is the temperature difference between the current and initial values; M_{CNT} and M_{CB} are mass ratio to cement of CNT and CB while the 100× values are used for reading friendly. For example, M_{CNT} and M_{CB} of T3B25 are 0.3 and 0.25, respectively.

The calculated results for sensitivity are shown in Fig. 9. Roughly, the extremely low content of additives cannot reach the threshold to build a conductive path, and this conclusion was valid for both CNT and CB. The effectiveness of CNT climbed up with the higher CB from B25 to B5. At the highest value of B75, the threshold of T1 was broken and jumped significantly over 50, but the benefit of T5 was impeded. T3 presented the optimal performance with B75 that reached around 100. Most powers of CB were covered up with T1, but T3 enabled all samples to show attractive results. The values of B25 and B5 doubled cooperated with T5, while the sensitivity of B75 declined by ~25 %. Increasing carbon additives raised the possibility of conductive path generation, while redundant nano materials disturbed particle distribution, leading to lower self-heating capability. T3B75 and T5B25 illustrated the

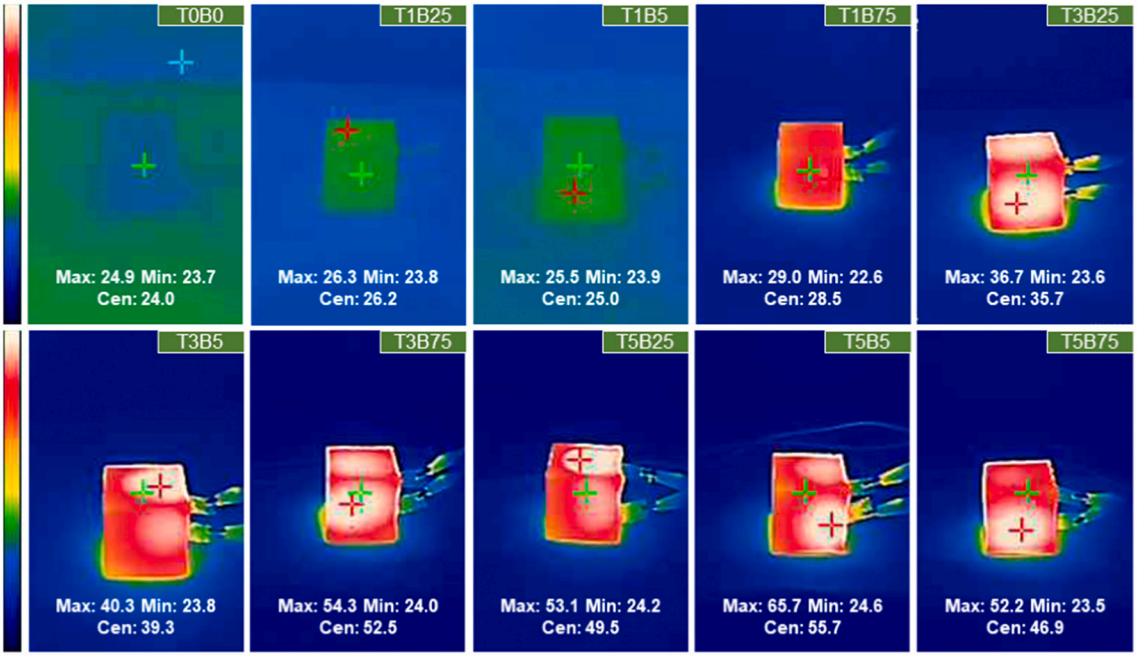

Fig. 6. Temperature distribution at 60 min after current application.

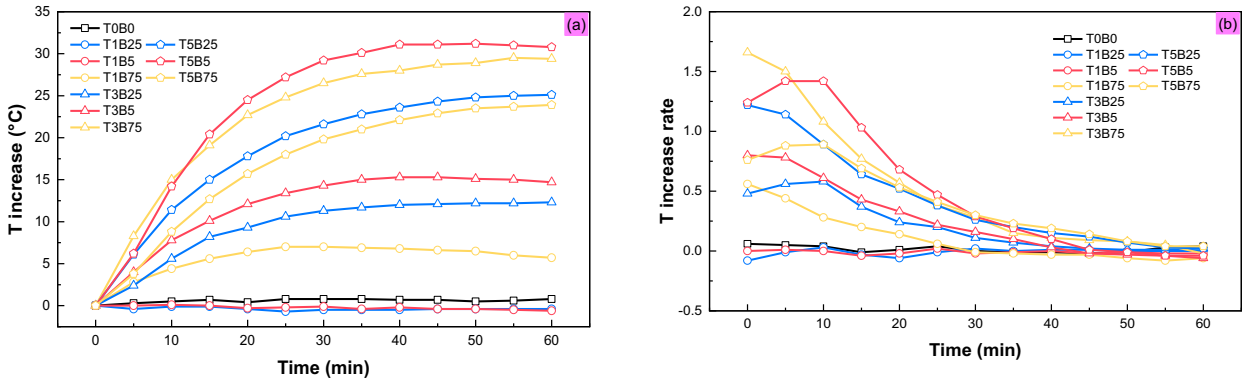

Fig. 7. Temperature profiles of central point along the time.

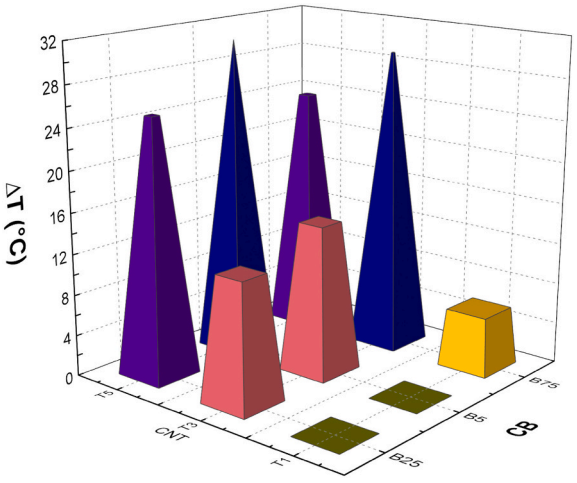

Fig. 8. One-hour temperature increase amplitude.

optimal efficiency of CNT and CB, respectively. A higher efficiency enabled less material consumption, less environmental burden, and lower cost. Combined with the result in Fig. 8, T3B75 offered the second highest temperature, and the gap compared to the highest value was very slight. The performance of T3B75 can be proposed as optimal comprehensively among the groups in this experiment.

4.2. Electrical conductivity

According to the Joule's Law, the higher electrical conductivity benefits higher power with the constant voltage. Concrete is typically non-conductive, so enhancing electrical conductivity is decisive, where lower electrical resistance helps to achieve better self-heating performance [10]. The electrical resistance (R) is a crucial factor in conductivity. The R-values at room temperature and 60 °C were tested separately, and the difference was analysed.

The normal mortar, T0B0, was not conductive, and temperature showed little effect on R. As shown in Fig. 10, the electrical resistance decreased obviously with the help of carbon additives [33]. T1B25 and T1B5 became conductive but still did not reach the threshold, although the R resistance loss was remarkable. T1B75 was the first sample showing self-heating ability with the R of ~1.5 kΩ, which could be regarded as the threshold in this experiment. Next, R of T3B25 and T3B5 dropped to around 250 Ω, leading to the double temperature increment in Fig. 8. With the further additive of T3B75, R fell continuously. However, R of T5 groups presented a relatively steady value. Compared with Fig. 8, the temperature increment and R had similar regulation and a great relationship. The samples can be classified into 5 groups: non-conductive (T0B0), conductive but without self-heating ability (T1B25 and T1B5), the threshold for self-heating (T1B75), moderate self-heating (T3B25 and T3B5), and ceiling self-heating (T3B75, T5B25, T5B5 and T5B75).

It is noticeable that all samples (except non-conductive T0B0) illustrate R reduction from the room at a higher temperature, which is attributed to the PCM state change. The PCM changed from solid to liquid state with temperature increasing, where the inorganic hydrated

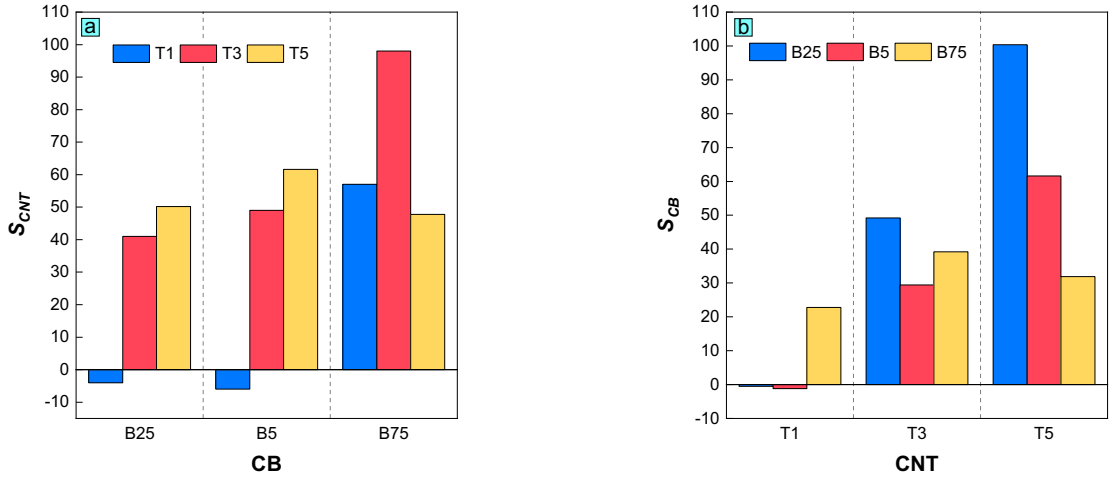

Fig. 9. Electrical sensitivity of tested carbon materials: (a) electrical sensitivity of CNT; (b) electrical sensitivity of CB.

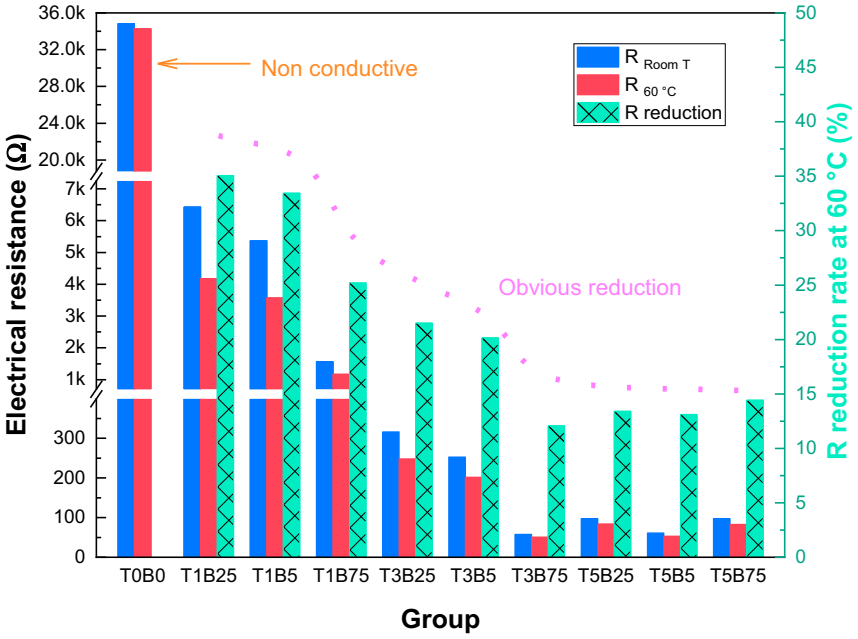

Fig. 10. Electrical resistance at different temperatures and changes.

salt was selected in this experiment. The EPC contained free ions in the liquid state, and the ionic liquid improved the electrical conductivity. As shown in Fig. 10, the *R* reduction of T1B25 was lower than 35 % while it went down with more carbon additives. The benefit of phase change of PCM on electrical conductivity was constant. Compared with significantly rising electrical conductivity caused by carbon additives, the advantage of PCM was relatively minor. With higher additive content, *R* reduction rate declined to 20 % for T3B5. Then, it showed fluctuation with a slight amplitude that was similar to the fluctuation of electrical conductivity. In summary, the melted inorganic hydrated salt is able to enhance electrical conductivity, but its effectiveness is limited, especially for the samples with great self-heating performance. This result was contributed to the feature of selected PCM. In another case, the paraffin-based PCM plays an adverse role in electrical conductivity improvement [31], which illustrates that the compatibility of PCM deserves much attention in future research.

4.3. Electrical impedance

4.3.1. Impedance spectroscopy

Fig. 11 presents the Nyquist plots of various groups. The plot of a plain PCM-filled sample (T0B0) contains a single high-frequency arc and a low-frequency arc. In contrast, the plots of other samples with carbon additives contain two high-frequency arcs and one low-frequency cycle, which is consistent with the typical plot characteristics of conductive cement-based composites. A partial high-frequency arc is not visible since the testing frequency is limited to 10 MHz. The high-frequency arcs are influenced by the conductive phase and matrix structure of the composites, and the low-frequency arc is related to the electrochemical behaviour of the electrode-specimen interface. Meanwhile, the arc diameter and the intersection of the high-frequency arc and electrode arc (corresponding to DC resistance) are incrementally decreased with the increasing contents of CNT or CB, which partially validate the obtained impedance spectrum.

It is seen that Nyquist plots are significantly influenced by the temperature. It has been proposed that the temperature has a complex influence on the electrical resistivity of the conductive cement-based composites through the charge carrier mobility, concentration, and intrinsic resistivity of the conductive fillers [40]. On the one hand, the increase in temperature leads to an enhancement in carrier transport current due to hole conduction [41]. On the other hand, the electrical properties of a cement composite are altered as a consequence of the difference in the thermal expansion coefficients between the conductive filler and the cement matrix [42]. It has been reported that the thermal expansion coefficient of cement is ten times higher than that of CNT [43]. It is noticeable that the impedance measurement was conducted on dried specimens to avoid the effect of free water; thus, the ionic conduction from pore solution contributed by free water is virtually eliminated. In this sense, the ionic conductivity contributed by the molten PCM could be easily differentiated.

4.3.2. Establishment of equivalent circuit

Referring to previous studies, the plain and conductive cementitious composites can be modelled with equivalent circuits of Q(RW)(Q(RW)) and Q(RW)(QR)(Q(RW)), respectively. The corresponding equivalent circuit elements and their associated physical meanings are illustrated in Fig. 12.

In general, the continuous conductive paths (CCP) comprise connected conductive elements, including connected conductive fillers and connected pores filled with pore solution, which act as resistance in the circuit. In contrast, the discontinuous conductive paths (DCP) comprise disconnected conductive fillers, and closed pores can be regarded as capacitances. In addition, the clumps of conductive fillers can be represented by a Resistance-Capacitance-Resistance circuit element, the resistance and capacitance conducted in series and in parallel. Because of the complex nature of pores, such as size, shape, moisture level, pore structure, etc., their time-constant response to various frequency ranges shows the discrepancy. Thus, pores cannot be regarded as a pure capacitor but instead as the constant phase elements (CPE, expressed by *Q*). The impedance of CPE is illustrated in Eq. (3)

$$Z_Q = \frac{1}{Y_0 \omega^n}\left(cos\frac{n\pi}{2} - jsin\frac{n\pi}{2}\right) \tag{3}$$

where Z_Q denotes the impedance (Ω); j is the imaginary unit; ω denotes the angular frequency (rad/s); Y_0 denotes the admittance; n is the parameter of CPE (CPE acts as a pure capacitor when $n = 1$; and CPE acts as a pure resistor when $n = 0$).

The formula for the total impedance of circuit model Q(RW)(QR)(Q(RW)) is illustrated in Eq. (4).

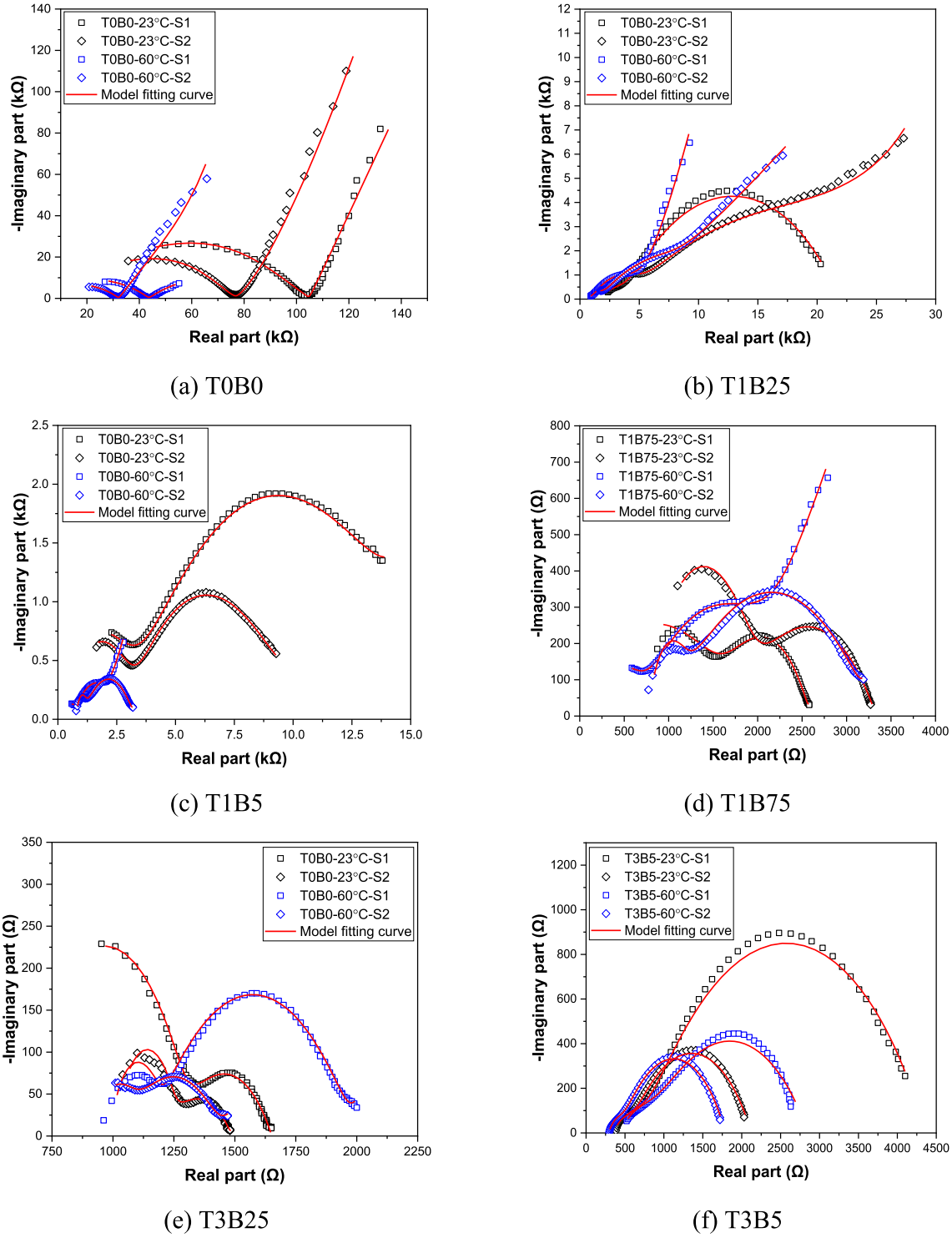

Fig. 11. Nyquist plots of the specimens.

$$Z = \frac{1}{\frac{1}{Z_{Q_1}} + \frac{1}{Z_{R_{ct1}} + Z_{W_1}}} + \frac{1}{\frac{1}{Z_{Q_N}} + \frac{1}{Z_{R_N}}} + \frac{1}{\frac{1}{Z_{Q_2}} + \frac{1}{Z_{R_{ct2}} + Z_{W_2}}}$$
$$= \frac{Z_{Q_1}\left(Z_{R_{ct1}} + Z_{W_1}\right)}{Z_{R_{ct1}} + Z_{W_1} + Z_{Q_1}} + \frac{Z_{Q_N} \times Z_{R_N}}{Z_{Q_N} + Z_{R_N}} + \frac{Z_{Q_2}\left(Z_{R_{ct2}} + Z_{W_2}\right)}{Z_{R_{ct2}} + Z_{W_2} + Z_{Q_2}} \quad (4)$$

where Q_N represents the constant phase element of conductive fillers (CB, CNT, CF); R_N represents the resistance of the CCP comprised of connected conductive fillers; R_{ct1} and R_{ct2} denote the electron transfer resistance in the cement matrix (mainly contributed by DCP) and the surface of electrodes, respectively; Q_1 denotes the constant phase element in the cement matrix; Q_2 denotes the constant phase element between the cement/conductive fillers and the electrodes; W_1 and W_2 are the Warburg resistance triggered by the electron diffusion in the cement pastes and the electrodes, respectively. The impedance formulas of W_1 and W_2 are displayed in Eqs. (5) and (6), respectively.

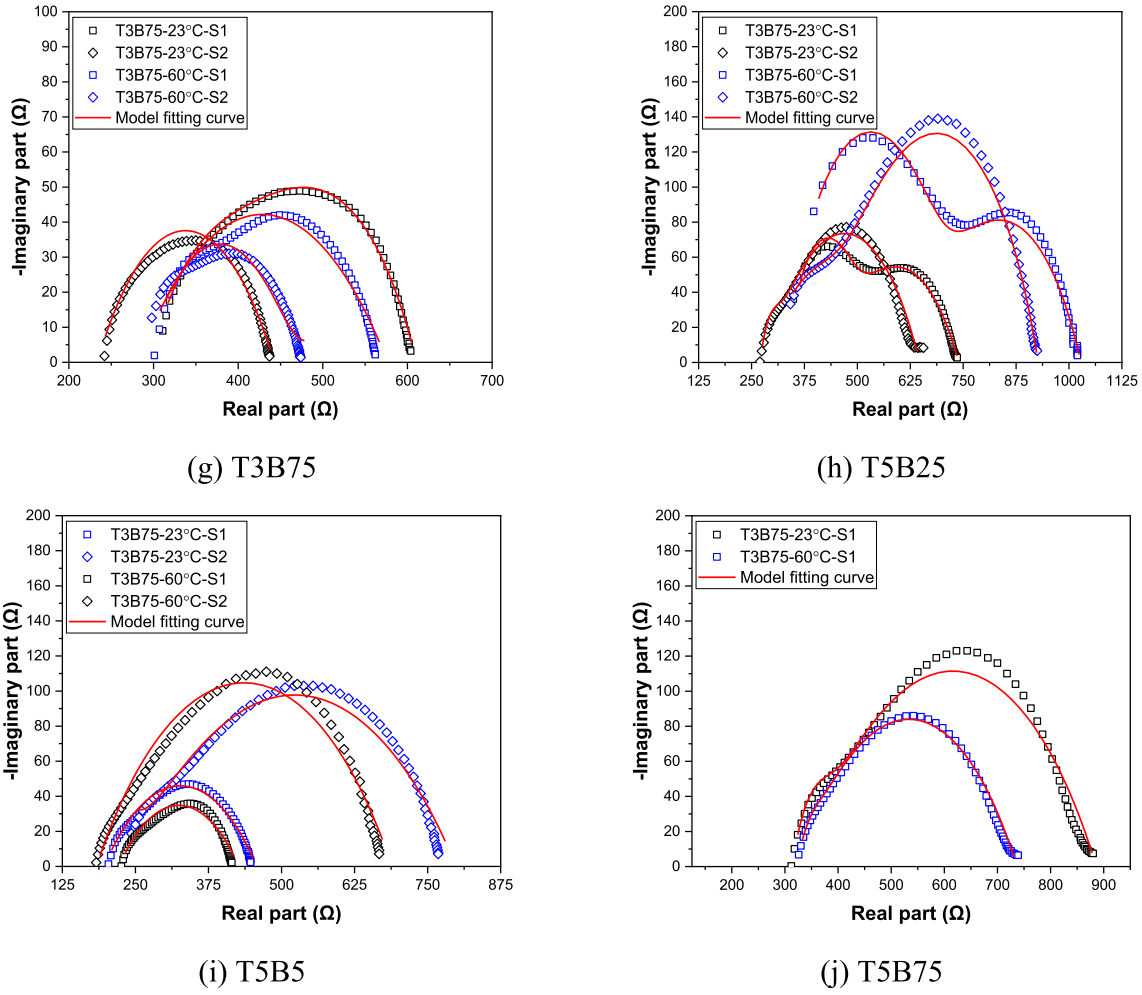

Fig. 11. (*continued*).

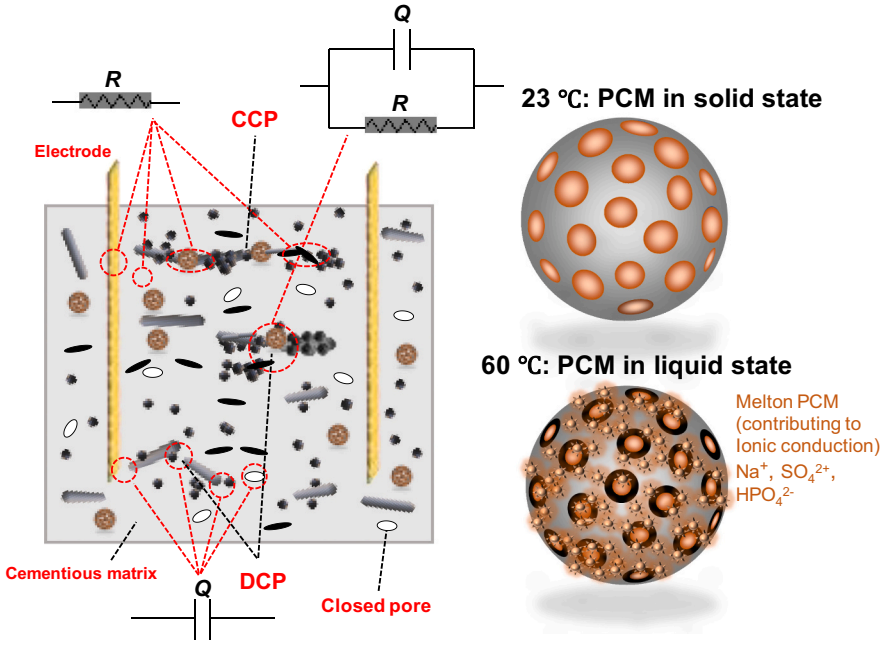

Fig. 12. Equivalent circuit elements and physical meanings.

$$Z_{W_1} = \frac{\sigma_1}{\sqrt{\omega}} - j\frac{\sigma_2}{\sqrt{\omega}} \quad (5)$$

$$Z_{W_2} = \frac{\sigma_2}{\sqrt{\omega}} - j\frac{\sigma_2}{\sqrt{\omega}} \quad (6)$$

Specific to this study, the electrical role of SSPCM is temperature-dependent. The PCM adopted in this study is eutectic hydrated salt with a melting point of approximately 28 °C. With the temperature increasing from 23 °C to 60 °C, the PCM transferred from solid to liquid state. Free ions, including Na^+, SO_4^{2+}, and HPO_4^{2-} were absorbed on the surface of open porosity. In addition, there is inevitably leakage of a minor quantity of PCM. The movement of these free ions surrounding the EP contributes to the ionic conduction, making it partially conductive. In other words, the inorganic hydrated salt PCM-impregnated EP alters to a 'semi-conductive aggregate' under 60 °C. Plenty of 'semi-conductive aggregate' broadly distributed in the cement matrix may act as conductive components contributing to either CCP or DCP [8].

4.3.3. Analysis of circuit parameters

The fitting curves of the proposed equivalent model are illustrated in Fig. 13. To analyse the influence mechanism of PCM on the electrical behaviour of multiple carbon additives filled mortar, the variations of two essential parameters R_N and R_{ct1}, which stand for CCP and DCP, respectively. Are illustrated in Fig. 14. With respect to plain group T0B0, there is a significant drop in R_1 by approximately 47.1 % when temperature increases from 23 °C to 60 °C. Since free water is eliminated in the specimens, the drop in R_1 is deduced to be mainly contributed by the SSPCM as semi-conductive aggregates in liquid state, which should validate the positive role of PCM in the liquated state in enhancing the conductivity of SSPCM. This hypothesis is further supported by the obvious drops in both R_N and R_{ct1} for the groups T1B25 and T1B5, where the CNT and CB contents are relatively low. In these cases, the thermal expansion coefficient has a limited effect on the electrical conductivity because of the less presence of conductive paths that are marginally distributed in the matrix. Therefore, the role of 'conductive' SSPCM in enriching the conductive passages is pronounced, actively contributing to the increase of both DCP and CCP, which shows a good agreement with simultaneous drops in R_N and R_{ct1} for the groups T1B25 and T1B5. On the contrary, it is seen that R_N under 60 °C is higher than that under 23 °C as the increases of CB and CNT contents, which is detected in the groups of T1B75, T3B5, and T5B75.

In these cases, due to the presence of rich conductive paths, the thermal expansion effect enlarges the potential barrier between adjacent fillers, thus impairing the continuity of conductive paths and leading to a positive temperature coefficient effect (PTC, the resistivity increases with increasing temperature). There are several exceptions, including T3B75, T5B5 and T5B75, wherein a significant drop in R_N was observed. Previous studies [9,42,44] proposed that the occurrence of the PTC effect required the degree of thermal expansion to reach a certain level, the thermal treatment of the present study (stored in a 60 °C oven for 3 h) should fulfil such thermal expansion degree. Compared to R_N, R_{ct1} is less varied for these groups from 23 °C to 60 °C. This suggests that thermal expansion mainly contributed to the reduction in length and continuity of CCP rather than the DCP. The value R_N under 60 °C is significantly higher than that under 23 °C for the composites with higher content of CNT or CB (T5 and B75 cluster groups), which follows the fact that the thermal expansion poses a more pronounced impact on CCP when abundant conductive paths are presented. Interestingly, for all B75 cluster groups, accompanied by the fact that R_N is significantly increased, R_{ct1} is significantly reduced when temperature increases from 23 °C to 60 °C, revealing the significant increase in length and continuity of DCP. Previous studies [45–47] proposed that loose and porous CB particles and their agglomerations are prone to absorb part of the free water in the cementitious matrix, which hindered the hydration process, thus resulting in an increase in porosity and reduced compactness in the cementitious matrix. Consequently, it is induced that the porous matrix is more prone to thermal expansion.

Yoon et al. [44] proposed that the physicochemical structure of the cement matrix, such as the generation of additional pores, expedited the PTC effect of conductive cementitious composite, as shown in Fig. 15. The pronounced thermal expansion of cement not only increases the discontinuity of CCP but also contributes to the increase in the number and length of DCP. For other groups, the variation of R_{ct1} is minor, evidencing less interference of DCP from the thermal expansion effect due to a more compact matrix. The significant variations of R_N and R_{ct1} in B75 cluster groups imply substantial alterations of both CCP and DCP in the composite, showing that the presence of a high content of CB can lead to significant temperature-dependent electrical characteristics of the composite. The temperature-dependent electrical behaviour is not ideal for the multifunctional cementitious composite, and thus, limiting the CB content is important.

4.3.4. Linkage to self-heating performance

The foregoing analysis indicates that the substantial CCP has been disconnected and evolved to DCP when temperature increases from 23 °C to 60 °C, and this effect initiates at the phase change point (28 °C).

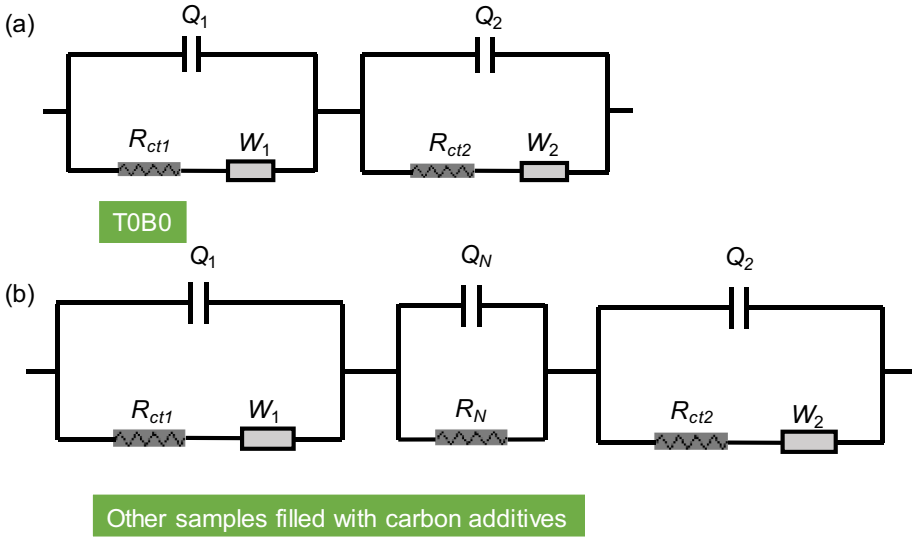

Fig. 13. Equivalent circuit models for specimens.

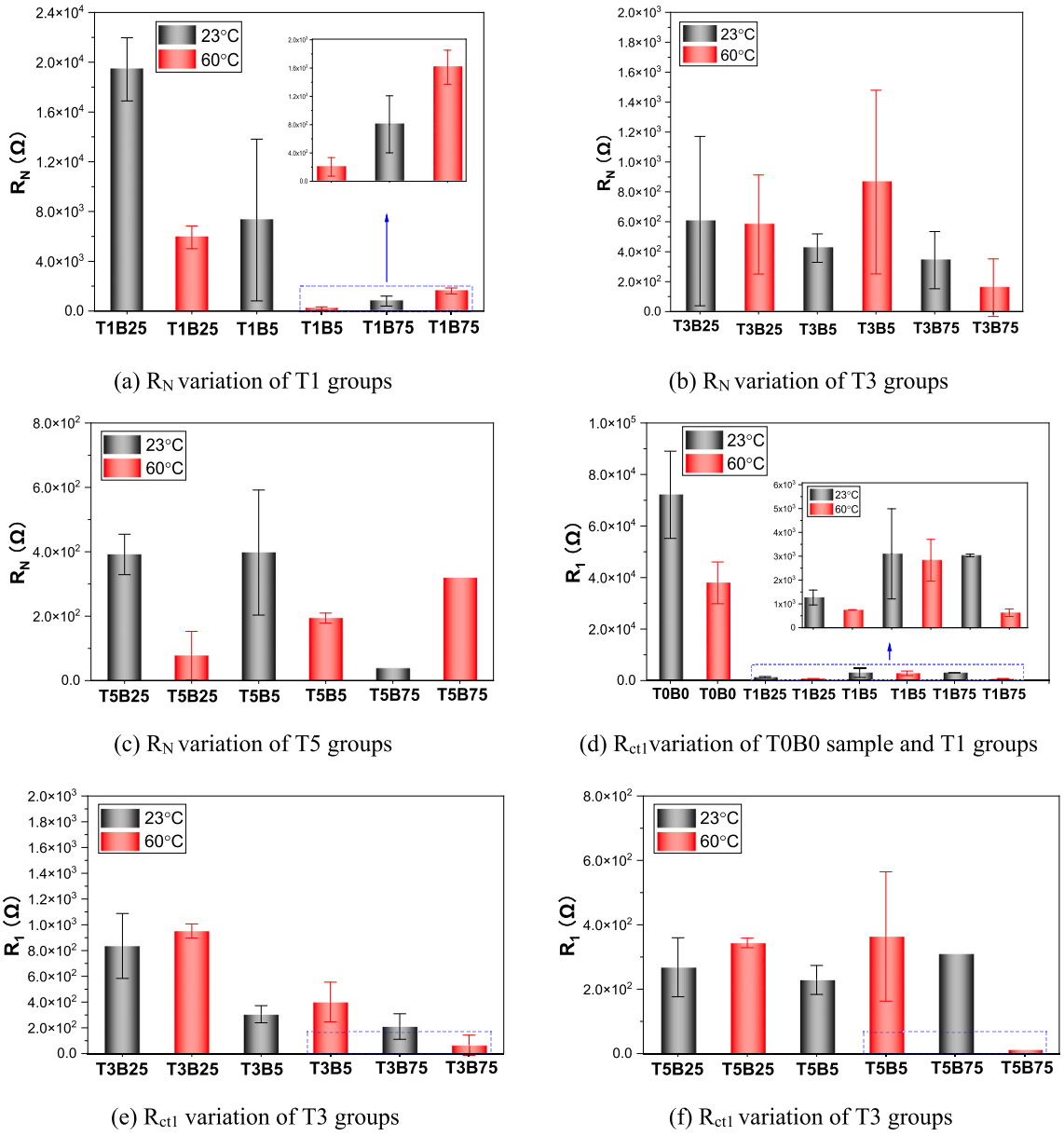

(a) R_N variation of T1 groups

(b) R_N variation of T3 groups

(c) R_N variation of T5 groups

(d) R_{ct1} variation of T0B0 sample and T1 groups

(e) R_{ct1} variation of T3 groups

(f) R_{ct1} variation of T3 groups

Fig. 14. Variations of R_N and R_{ct1}.

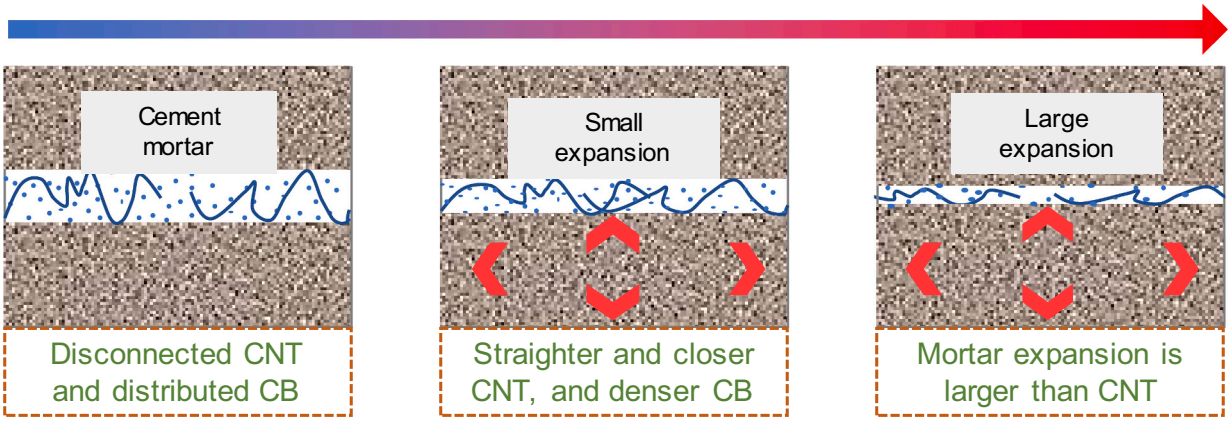

Fig. 15. Effect of thermal expansion on conductive paths [9].

This could interpret the fact that although the conductivity of T5B75 is comparable to T5B25, T5B5 and T3B75. T5B75 exhibits obviously inferior self-heating performance compared to them. Conversely, T3B75, T5B25 and T5B5 manifest a significant drop in R_N and a margin increase in R_{ct1} when temperature increases from 23 °C to 60 °C, implying that the amelioration effect of the increase in CCP initiating at the phase change point (28 °C), which is well aligned with the superior heating performance of T5B25 against T5B5 and T5B5 against T5B75. The good coincidence between the analytic results induced from the equivalent circuit model and macro self-heating performance should prove the validity of the proposed model.

4.4. FTIR

The chemical component is illustrated in Fig. 16. The expected peaks for cement hydration products are found such as Si—O. Compared with reference group T0B0, all samples have a similar FTIR spectrum model. The small number of additives reduces the noise, but superfluous additives increase it again to a worse state. The main peaks are observed, and there is no new peak. It is generally concluded that the modification of PCM and carbon additives does not change the chemical components of the designed mortar.

4.5. Microstructure (SEM)

The microstructure of hydration products with varying additive distribution establishes the electrically conductive path. That directly determines the electrical resistance, affecting the self-heating ability. Many SEM pictures were taken to investigate the changing microstructure of PCM mortar.

Similar to universal cement-based materials, C-S-H, portlandite, and ettringite are found in Fig. 17(a), which are stacked or connected. These materials have very high electrical resistance. A lot of pores and cracks are obvious that aggravate the bad electrical conduction. With the carbon additive, the conductive path is possible. As shown in Fig. 17(b), CF is long enough to bridge cracks to eliminate the adverse influence of pores and cracks. Nano-scale additives are distributed in cement paste to enhance its electrical conductivity. Cementitious products wrap CF, providing many contact points, which enables the establishment of whole conductive samples. The higher proportion of additives offers a higher possibility of a long conductive path, which is effective in electrical circuits and electrical networks.

With the increasing content of conductive additives, increased electrical conduction is achieved. As shown in Fig. 18, CNT is integrated with various hydration products, including C-S-H, portlandite, and ettringite. The well-distributed CNT plays a significant role in changing the cement matrix from non-conductive to conductive. At a high magnification of 20 k, a cluster of CNT is remarkable, and CB is scattered. CB is found on the surface of small C-S-H, providing a large conductive surface connected with CNT, which benefits the building of an electrical network. At the same time, CB and CNT are engaged with C-S-H in different ways, such as wrapping, adhering, and connecting. The mixed coexist formation allows conductive additives to improve the electrical properties of cement matrix from multi-scale. The cement matrix is the critical part of integrating all components like aggregate and fibre. Therefore, enhancing the cement matrix contributed by nano-additives is significant for the comprehensive performance, in addition to the millimetre additives like CF.

The advantages of nano-additives have been proven, but it is hard to achieve optimal results because the operation and control are difficult. As shown in Fig. 19, additives are obvious. At a large magnification of 30 k, the uneven distribution is clear. CNT is prone to agglomeration as a large group, and rich CB is scattered everywhere. The imperfect dispersion of raw materials is one reason. In addition, the electric charge and the interaction force of the large surface aggravated the agglomeration level. Hydration products, like C-S-H, still show a stable connection with additives. Although the C-S-H with rich additives has excellent electrical conductivity, the whole electrical network is broken. The benefit of CNT length is restricted, leading to less conductive connection. The self-heating ability relies on restrained electrical circuits. On the other hand, agglomeration mainly affects CNT morphology, stretch, and distribution. This defect has little influence on CB but is still effective in enhancing the electrical properties of hydration products. CNT and CB should cooperate in optimal content.

5. Conclusions

This paper presents the design of self-heating cementitious mortar incorporating PCM. This multifunctional mortar has a brilliant self-heating ability in a modified PCM mortar. This study provides significant findings in the development of additional functions based on PCM mortar. Several conclusions are given below:

(1) Universal mortar is not electrically conductive, while carbon additives can significantly enhance it to achieve self-heating performance. In this experiment, T3B75 and T5B5 have the best

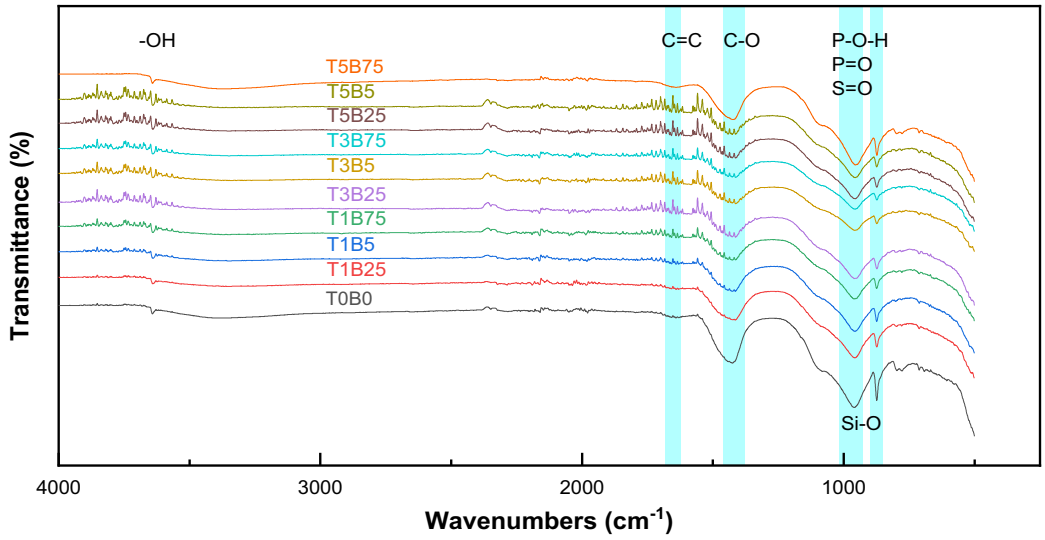

Fig. 16. FTIR for samples after 28-day curing.

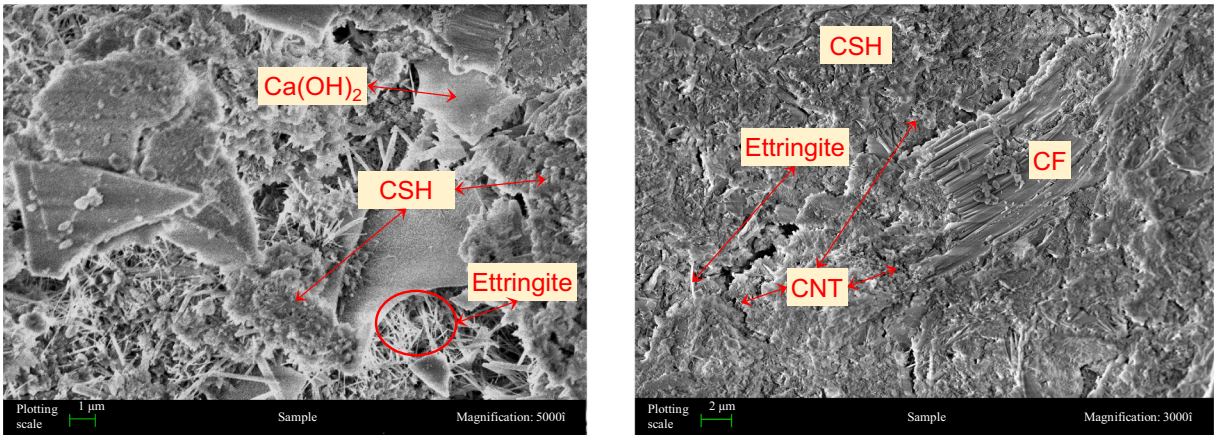

(a) T0B0 without additives (b) T1B5 with additives

Fig. 17. Microstructure of hydration products with varying additive.

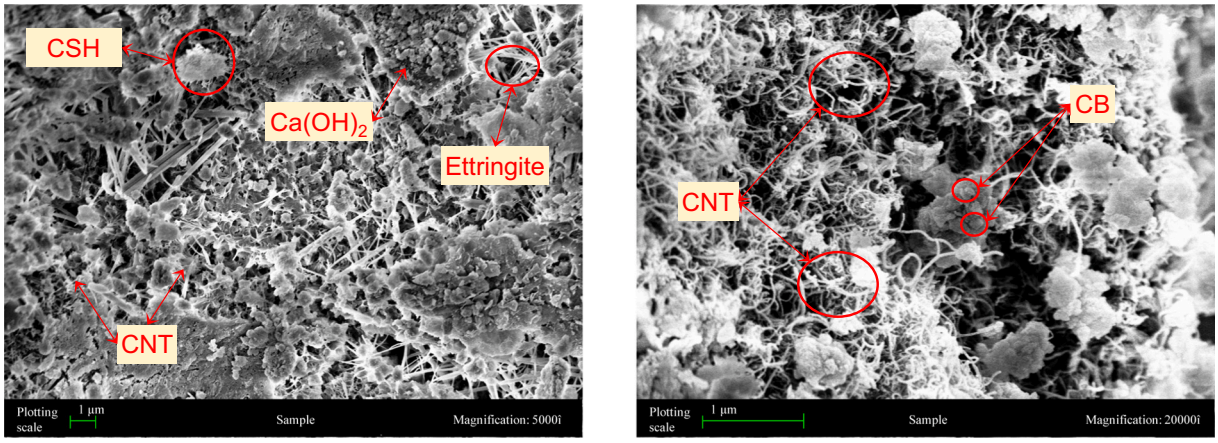

Fig. 18. Microstructure of T3B75 with well-distributed additives.

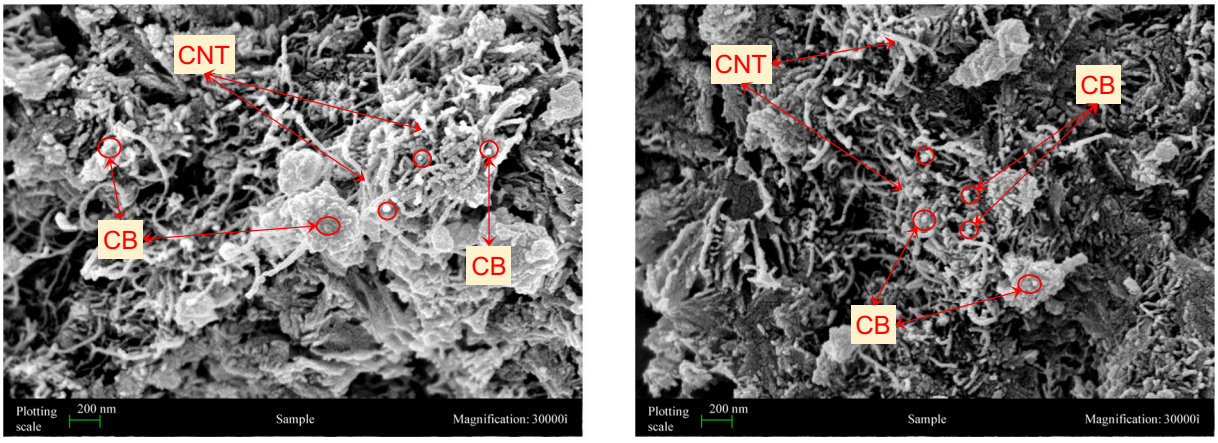

Fig. 19. Microstructure of T5B5 showing additive aggregation.

electrical conductivity with the same content of CF, when the optimal result reaches around 50 Ω. The drop in electrical resistance is remarkable over 80 %, even for the sample with the lowest additives. The reduced electrical resistance is closely related to improved self-heating efficiency.

(2) T1B25 and T1B5 do not show any increasing temperature, although their electrical resistance declines significantly by ~80 % than T0B0. Their currency is not enough to generate thermal energy and is captured by the mortar. T1B75 has an obvious self-heating performance with the lowest additives that show a

temperature increment lower than 5 °C. It is regarded as the threshold in this experiment.

(3) The sensitivity of CB and CNT is different and mutually affecting. In most samples, the higher content of one material will benefit the effectiveness of the other material. The optimal sensitivity of CB is incorporated with B75, and the CNT counterpart occurs with T5. The proposed sample, T3B75, takes the full power of CNT and presents a significant advantage of CB.

(4) Considering the electrical conductivity and SEM results, CF can bridge most cracks and pores while CB and CNT modify the micro properties. Although both nano-additives improve the electrical conductivity, CNT has better connection performance due to its larger aspect ratio. CB is prone to incorporate (wrap and attach) hydration products.

(5) At the temperature over the melting point of PCM, the electrical conductivity is increased at various rates. With higher content carbon additives, the improvement effectiveness caused by PCM is weaker. However, the lowest improvement rate still reached 10 %. Melted PCM is a rich ion solution in this experiment that provides free ions for electron transmission.

(6) A novel Q(RW)(QR)(Q(RW)) equivalent circuit model is proposed to understand the electrical behaviors during the self-heating process, which is verified by the good fitting degree with varying model parameters. The analytic results from the latter show an excellent coincidence with macro self-heating performance.

CRediT authorship contribution statement

Xiaonan Wang: Writing – review & editing, Writing – original draft, Validation, Methodology, Investigation. **Yipu Guo:** Writing – review & editing, Writing – original draft, Validation, Investigation. **Zhong Tao:** Writing – review & editing, Writing – original draft, Validation, Supervision. **Long Shi:** Writing – review & editing, Writing – original draft, Validation. **Wengui Li:** Writing – review & editing, Writing – original draft, Visualization, Supervision, Resources, Methodology.

Declaration of competing interest

The authors declare that they have no known competing financial interests or personal relationships that could have appeared to influence the work reported in this paper.

Acknowledgements

The authors would like to acknowledge the support from the Australian Research Council (ARC), Australia (FT220100177, LP230100288, DP220101051, DP220100036 and IH200100010). Xiaonan Wang also thanks the support from China Scholarship Council (CSC).

Data availability

Data will be made available on request.

References

[1] J. Gomis, O. Galao, V. Gomis, E. Zornoza, P. Garcés, Self-heating and deicing conductive cement. Experimental study and modeling, Constr. Build. Mater. 75 (2015) 442–449.
[2] M.L. Rahman, A. Malakooti, H. Ceylan, S. Kim, P.C. Taylor, A review of electrically conductive concrete heated pavement system technology: from the laboratory to the full-scale implementation, Construct. Build Mater. 329 (2022) 127139.
[3] J. Cai, X. Li, J. Tan, B. Vandevyvere, Fly ash-based geopolymer with self-heating capacity for accelerated curing, J. Clean. Prod. 261 (2020) 121119.
[4] A.A. Moman, A.A. Butt, S. Nassiri, Feasibility assessment of self-deicing concrete pavements with recycled CFRP reinforcement: environmental and mechanical performance, Resour. Conserv. Recycl. 198 (2023) 107213.
[5] M.K. Hassanzadeh-Aghdam, M.J. Mahmoodi, M. Safi, Effect of adding carbon nanotubes on the thermal conductivity of steel fiber-reinforced concrete, Compos. Part B Eng. 174 (2019) 106972.
[6] W. Li, W. Dong, Y. Guo, K. Wang, S.P. Shah, Advances in multifunctional cementitious composites with conductive carbon nanomaterials for smart infrastructure, Cement Concr. Compos. 128 (2022) 104454.
[7] Y. Guo, W. Li, W. Dong, Z. Luo, F. Qu, F. Yang, K. Wang, Self-sensing performance of cement-based sensor with carbon black and polypropylene fibre subjected to different loading conditions, J. Build. Eng. 59 (2022) 105003.
[8] D. Lu, Y. Huo, Z. Jiang, J. Zhong, Carbon nanotube polymer nanocomposites coated aggregate enabled highly conductive concrete for structural health monitoring, Carbon 206 (2023) 340–350.
[9] G.M. Kim, F. Naeem, H.K. Kim, H.K. Lee, Heating and heat-dependent mechanical characteristics of CNT-embedded cementitious composites, Compos. Struct. 136 (2016) 162–170.
[10] H. Lee, W. Yu, K.J. Loh, W. Chung, Self-heating and electrical performance of carbon nanotube-enhanced cement composites, Construct. Build Mater. 250 (2020) 118838.
[11] D. Jang, H.N. Yoon, J. Seo, S. Park, Enhanced electrical heating capability of CNT-embedded cementitious composites exposed to water ingress with addition of silica aerogel, Ceram. Int. 48 (9) (2022) 13356–13365.
[12] V. Kočí, M. Petříková, J. Fořt, L. Fiala, R. Černý, Preparation of self-heating alkali-activated materials using industrial waste products, J. Clean. Prod. 260 (2020) 121116.
[13] L. Fiala, M. Petříková, W.-T. Lin, L. Podolka, R. Černý, Self-heating ability of geopolymers enhanced by carbon black admixtures at different voltage loads, Energies 12 (21) (2019) 4121.
[14] S.M.S. Sadati, K.S. Cetin, H. Ceylan, S. Kim, Energy-efficient design of a carbon fiber-based self-heating concrete pavement system through finite element analysis, Clean Techn. Environ. Policy 22 (5) (2020) 1145–1155.
[15] C. Farcas, O. Galao, R. Navarro, E. Zornoza, F.J. Baeza, B. Del Moral, R. Pla, P. Garcés, Heating and de-icing function in conductive concrete and cement paste with the hybrid addition of carbon nanotubes and graphite products, Smart Mater. Struct. 30 (4) (2021) 045010.
[16] S. Gwon, H. Kim, M. Shin, Self-heating characteristics of electrically conductive cement composites with carbon black and carbon fiber, Cement Concr. Compos. 137 (2023) 104942.
[17] S. Gwon, J. Moon, M. Shin, Self-heating capacity of electrically conductive cement composites: effects of curing conditions, Construct. Build Mater. 353 (2022) 129087.
[18] Z. Wang, Z. Wang, M. Ning, S. Tang, Y. He, Electro-thermal properties and Seebeck effect of conductive mortar and its use in self-heating and self-sensing system, Ceram. Int. 43 (12) (2017) 8685–8693.
[19] M. Abedi, U. Kiran Sanivada, S. Ali Mirian, O. Hassanshahi, K. Al-Jabri, A. Gomes Correia, P.B. Lourenço, R. Fangueiro, A self-sensing and self-heating planar braided composite for smart civil infrastructures reinforcement, Construct. Build Mater. 387 (2023) 131617.
[20] B. Yu, S. Li, H. Zhu, Q. Jiang, D. Wang, Y. Chen, A composite phase change material for improving the freeze–thaw resistance performance of cement mortars, Construct. Build Mater. 387 (2023) 131657.
[21] D. Kumar, M. Alam, J. Sanjayan, Experimental and numerical investigation of novel light weight concrete panels made with aerogel and phase change materials, Energ. Buildings 283 (2023) 112836.
[22] M. Sawadogo, F. Benmahiddine, A.E.A. Hamami, R. Belarbi, A. Godin, M. Duquesne, Investigation of a novel bio-based phase change material hemp concrete for passive energy storage in buildings, Appl. Therm. Eng. 212 (2022) 118620.
[23] C. Li, X. Wen, W. Cai, J. Wu, J. Shao, Y. Yang, H. Yu, D. Liu, M. Wang, Energy performance of buildings with composite phase-change material wallboards in different climatic zones of China, Energ. Buildings 273 (2022) 112398.
[24] F. Kocyigit, M. Bayram, G. Hekimoglu, V.V. Cay, O. Gencel, A. Ustaoglu, A. Sarı, E. Erdogmus, T. Ozbakkaloglu, Thermal energy saving and physico-mechanical properties of foam concrete incorporating form-stabilized basalt powder/capric acid based composite phase change material, J. Clean. Prod. 414 (2023) 137617.
[25] X. Wang, W. Li, Z. Luo, K. Wang, S.P. Shah, A critical review on phase change materials (PCM) for sustainable and energy efficient building: design, characteristic, performance and application, Energ. Buildings 260 (2022) 111923.
[26] X. Wang, W. Li, Y. Huang, S. Zhang, K. Wang, Study on shape-stabilised paraffin-ceramsite composites with stable strength as phase change material (PCM) for energy storage, Construct. Build Mater. 388 (2023) 131678.
[27] H. Yang, Z. Xu, H. Cui, X. Bao, W. Tang, G. Sang, X. Chen, Cementitious composites integrated phase change materials for passive buildings: an overview, Construct. Build Mater. 361 (2022) 129635.
[28] A.K. Dubey, J. Sun, T. Choudhary, M. Dash, D. Rakshit, M.Z. Ansari, S. Ramakrishna, Y. Liu, H.S. Nanda, Emerging phase change materials with improved thermal efficiency for a clean and sustainable environment: an approach towards net zero, Renew. Sustain. Energy Rev. 182 (2023) 113421.
[29] A. Yousefi, W. Tang, M. Khavarian, C. Fang, Effects of thermal conductive fillers on energy storage performance of form-stable phase change material integrated in cement-based composites, Appl. Therm. Eng. 212 (2022) 118570.
[30] C. Li, X. Wen, W. Cai, H. Yu, D. Liu, Phase change material for passive cooling in building envelopes: a comprehensive review, J. Build. Eng. 65 (2023) 105763.
[31] D. Jang, H.N. Yoon, B. Yang, H.R. Khalid, Cyclic heat-generation and storage capabilities of self-heating cementitious composite with an addition of phase change material, Construct. Build Mater. 369 (2023) 130512.

[32] D. Niu, T. Zhang, X. Zhang, Y. Tan, W. Zhang, Experimental and numerical investigation of the thermal performance of phase-change module using built-in electrical heating, Energ. Buildings 299 (2023) 113597.
[33] Z. Wang, T. Shao, H. Zhang, J. Huo, J. Liu, T. Zhang, X. Ji, H. Zhang, J. Wang, H. Guo, P. Yu, Principles, properties and applications of smart conductive cement-based composites: a state-of-the-art review, Construct. Build Mater. 408 (2023) 133569.
[34] M. Ramezani, A. Dehghani, M.M. Sherif, Carbon nanotube reinforced cementitious composites: a comprehensive review, Construct. Build Mater. 315 (2022) 125100.
[35] M.N. Islam, D.H. Ahmed, Delaying the temperature fluctuations through PCM integrated building walls—room conditions, PCM placement, and temperature of the heat sources, Energy Storage 3 (5) (2021) e245.
[36] J. Hirschey, M. Goswami, D.O. Akamo, N. Kumar, Y. Li, T.J. LaClair, K. R. Gluesenkamp, S. Graham, Effect of expanded graphite on the thermal conductivity of sodium sulfate decahydrate (Na2SO4·10H2O) phase change composites, J. Energy Storage 52 (2022) 104949.
[37] Y. Fang, J. Su, Y. Tang, X. Liang, S. Wang, X. Gao, Z. Zhang, Form-stable Na2SO4·10H2O-Na2HPO4·12H2O eutectic/hydrophilic fumed silica composite phase change material with low supercooling and low thermal conductivity for indoor thermal comfort improvement, Int. J. Energy Res. 44 (4) (2020) 3171–3182.
[38] ASTM, C109/C109M - 21 Standard Test Method for Compressive Strength of Hydraulic Cement Mortars (Using 2-in. Or [50 Mm] Cube Specimens), ASTM International, West Conshohocken, PA, 2021.
[39] W. Dong, W. Li, X. Zhu, D. Sheng, S.P. Shah, Multifunctional cementitious composites with integrated self-sensing and hydrophobic capacities toward smart structural health monitoring, Cement Concr. Compos. 118 (2021) 103962.
[40] H. Qin, S. Ding, A. Ashour, Q. Zheng, B. Han, Revolutionizing infrastructure: the evolving landscape of electricity-based multifunctional concrete from concept to practice, Prog. Mater. Sci. 145 (2024) 101310.
[41] H. Wang, A. Zhang, L. Zhang, Q. Wang, X.-H. Yang, X. Gao, F. Shi, Electrical and piezoresistive properties of carbon nanofiber cement mortar under different temperatures and water contents, Construct. Build Mater. 265 (2020) 120740.
[42] G.M. Kim, S.M. Park, G.U. Ryu, H.K. Lee, Electrical characteristics of hierarchical conductive pathways in cementitious composites incorporating CNT and carbon fiber, Cem. Concr. Compos. 82 (2017) 165–175.
[43] E.J. Sellevold, Ø. Bjøntegaard, Coefficient of thermal expansion of cement paste and concrete: mechanisms of moisture interaction, Mater. Struct. 39 (9) (2006) 809–815.
[44] H.N. Yoon, J. Bang, D. Jang, B. Yang, Investigation on NTC/PTC effects of cement-based self-heating composites with varied conductive filler contents, Developments in the Built Environment 18 (2024) 100416.
[45] W. Li, Y. Guo, X. Zhang, W. Dong, X. Li, T. Yu, K. Wang, Development of self-sensing ultra-high-performance concrete using hybrid carbon black and carbon nanofibers, Cement Concr. Compos. 148 (2024) 105466.
[46] G. Gu, T. Ma, F. Chen, C. Han, H. Li, F. Xu, Co-modifying geopolymer composite by nano carbon black and carbon fibers to reduce CO2 emissions in airport pavement induction heating, Compos. A: Appl. Sci. Manuf. 177 (2024) 107951.
[47] Q. Zhang, C. Luan, C. Yu, Y. Huang, Z. Zhou, Mechanisms of carbon black in multifunctional cement matrix: hydration and microstructure perspectives, Construct. Build Mater. 346 (2022) 128455.